Two-dimensional Mn structure on the GaN growth surface and evidence for room-temperature spin ordering

Kangkang Wang,[1] Noboru Takeuchi,[1,2] Abhijit V. Chinchore,[1] Wenzhi Lin,[1] Yinghao Liu,[1,*] and Arthur R. Smith[1,†]

[1]*Department of Physics and Astronomy, Nanoscale and Quantum Phenomena Institute, Ohio University, Athens, Ohio 45701, USA*

[2]*Centro de Nanociencias y Nanotecnología, Universidad Nacional Autónoma de México, Apartado Postal 14, Ensenada Baja California, Codigo Postal 22800, Mexico*

(Received 25 January 2011; published 8 April 2011)

A class of striped superstructures with local hexagonal ordering has been obtained by depositing submonolayer Mn on the GaN(0001) surface. Combining scanning tunneling microscopy and first-principles theory, we find that Mn atoms incorporate into the surface and form a high-density two-dimensional Mn_xGa_{1-x} structure. The highly spin-polarized Mn *d* electrons are found to dominate the surface electronic states. For the narrowest stripes, we calculate a row-wise antiferromagnetic ground state, which is observed in real space at room temperature as a spin-induced asymmetry in the density of states. These two-dimensional magnetic structures on GaN can also be considered model systems for wide-band-gap magnet/semiconductor spin injectors.

DOI: 10.1103/PhysRevB.83.165407 PACS number(s): 68.35.bg, 68.37.Ef, 75.50.Pp, 75.70.−i

I. INTRODUCTION

Two-dimensional (2D) crystalline materials, often demonstrating unique and exceptional properties not existing in bulk, have gained tremendous interest in recent years because of their potential for revolutionizing current technology. While much research has focused on graphene, transition-metal based 2D structures have also been a topic of hot interest since the interplay among exchange, spin-orbit, Rudel-Kittel-Kasuya-Yosida, and magnetostatic interactions at a reduced dimension can result in novel electronic and spin structures.[1] For example, a chiral spin spiral has been observed for a single Mn layer on W(110),[2] 2D spin-glass ordering was reported for submonolayer Fe on InAs,[3] and giant magnetic anisotropy has been studied in $Fe_{50}Pt_{50}$ surface alloys.[4]

Here, we report a class of 2D striped structures obtained by depositing submonolayer Mn on the GaN(0001) surface. Using scanning tunneling microscopy (STM) and first-principles theory, an atomic structural model is discovered consisting of a high-density 2D Mn_xGa_{1-x} surface layer with local $\sqrt{3}\times\sqrt{3}$-*R*30° ordering. The highly spin-polarized Mn *d* electrons are shown to dominate the surface electronic density, which results in direct identification of Mn atomic sites within the 2D structures. In addition, an antiferromagnetic (AFM) spin alignment is observed for one of the phases due to a spin-induced asymmetry in the electronic structure.

Since Heusler-type Mn-Ga alloys exhibit many magnetic phases ranging from ferromagnetic to ferrimagnetic and antiferromagnetic,[5–8] we propose that the obtained structures form a model system for exploring crossovers between different 2D magnetic phases. Furthermore, the abrupt interface between the 2D layer and its substrate, along with the highly spin-polarized *d* electrons, make this system of high interest for spin injection into wide band-gap semiconductors.

II. EXPERIMENTS

Experiments are carried out in an ultrahigh-vacuum plasma-assisted molecular-beam-epitaxy (MBE) STM chamber system. Commercially available metal-organic chemical-vapor deposition grown GaN(0001) wafers are solvent cleaned *ex situ* and then annealed *in situ* at 650 °C under nitrogen plasma. MBE GaN growth is carefully maintained at Ga-rich conditions resulting in smooth spiral mode growth, while at the same time, avoiding Ga droplet formation.[9] After growing ∼100 nm of GaN, the substrate temperature is then lowered to ∼250 °C for Mn deposition. The entire growth and deposition process is monitored by reflection high-energy-electron diffraction (RHEED). After Mn deposition, the samples are immediately transferred *in situ* to the analysis chamber for a room-temperature-STM investigation. Alternating-current-etched and electron-beam-annealed W tips are used in this study. Tunneling conductance spectra are taken via a lock-in method where a small sinusoidal modulation voltage is added to the sample bias.

III. RESULTS AND DISCUSSIONS

A. Experimental observation of the stripe phases

Figure 1 shows the RHEED evolution upon depositing up to 0.5 monolayer (ML) of Mn onto GaN(0001). Clear "1×1" ($1+\frac{1}{6}$) streaks along [11$\bar{2}$0] [see Fig. 1(b)] are observed before deposition, indicating the existence of fluidic Ga bilayer-covered terraces.[9,10] No apparent fractional streaks are found along [11$\bar{2}$0] with Mn deposition. On the other hand, significant changes are observed along [1$\bar{1}$00]. At lower than 0.3-ML coverage [see Fig. 1(c)], a split fractional streak slightly outside the $\frac{2}{3}$ order position is observed. Approaching 0.5-ML coverage [see Fig. 1(d)], the split streak slowly merges and shifts toward the $\frac{2}{3}$ position, together with the emergence of a weak $\frac{1}{3}$ streak. An evolution of the line profile as a function of coverage is shown in Fig. 1(e). These clear fractional streaks indicate well-ordered superstructures developed on the GaN surface.

At lower than 0.3-ML-Mn coverage, the surface is found to consist of stripe reconstructed terraces which occur in localized areas surrounded by a sea of featureless 1×1 terraces. Mn atoms evidently have a high mobility within the 1×1 surface, tending to aggregate into a few large, rather than many small, reconstructed areas. Figure 2(a) shows a representative STM image of such reconstructed terraces. Two stripe phases along $[1\bar{1}00]_{GaN}$ are clearly observed at this coverage, one with a narrower row-row spacing denoted as the α phase, and the other with a wider row-row spacing denoted as the β phase.

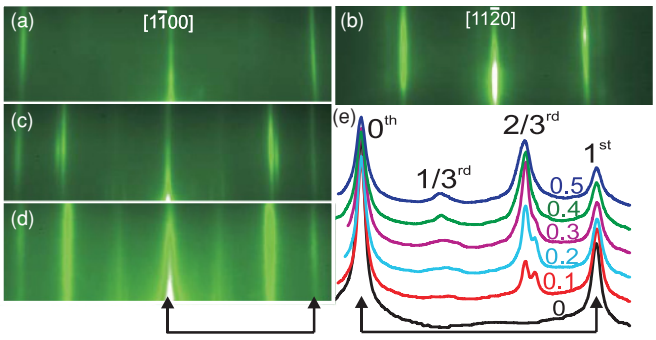

FIG. 1. (Color online) RHEED evolution during Mn deposition. (a), (b) Starting a GaN(0001)-1 × 1 surface. (c), (d) After depositing 0.3 and 0.5 ML of Mn, respectively; taken along $[1\bar{1}00]_{GaN}$. (e) Stacked line profiles along $[1\bar{1}00]$ (right half) as a function of Mn coverage.

While the two phases are found to coexist at this coverage, here we only discuss details of the α phase since it represents the narrowest limit of the stripe class. Figure 2(b) shows a closeup of the α phase with atomic resolution showing a clear zigzag row structure. The unit cell [black box in Fig. 2(b)] for the α phase is then determined to be $4a$ along $[11\bar{2}0]$ and $\sqrt{3}a$ along $[1\bar{1}00]$, a being the lattice constant of bulk GaN (3.189 Å).

Approaching 0.5-ML-Mn coverage, the surface is mostly reconstructed showing wide stripes running along the three equivalent directions of $\langle 1\bar{1}00\rangle$ (referred to as the γ phase). Figure 2(c) shows a STM image of two neighboring reconstructed terraces with γ-phase domains 120° apart. The stripes

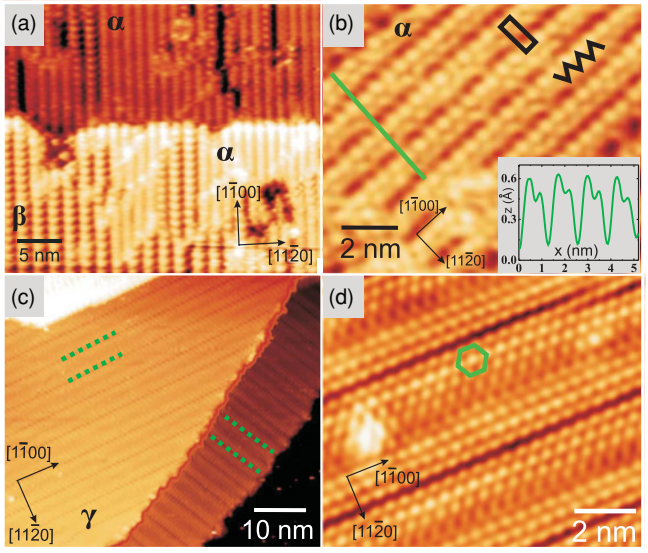

FIG. 2. (Color online) (a) Representative STM image showing coexistence of α and β phases at ~0.2-ML-Mn coverage. (b) Closeup of the α phase. Inset: Averaged line profile along green line. Both: $V_s = -0.4$ V and $I_t = 0.2$ nA. (c) Neighboring terraces having γ-phase reconstructions. Dotted green lines are for visual guidance. (d) Closeup of the left terrace in (c). Both: $V_s = -1.0$ V and $I_t = 0.1$ nA. Local contrast has been applied for better presentation in (a) and (c).

are separated by sharp trench lines. A closeup is shown in Fig. 2(d) where a local $\sqrt{3}\times\sqrt{3}$-$R30°$ structure is identified. In this particular case, each stripe consists of either eight or nine atomic rows, but stripes with other widths (4–6, >10) are also observed.

These observed stripe phases existing over a wide range of Mn coverage clearly form an important class of Mn superstructures on the GaN surface. The class is defined by the common directionality as well as a common local geometry within the stripes. Given that the α phase is the lower limit of the stripe class with a domain width of two atomic rows, the γ phase can then be seen as approaching the upper limit—a complete $\sqrt{3}\times\sqrt{3}$-$R30°$ layer.

B. Computational details

To further unravel the atomic structures of these stripe phases, we have carried out calculations in the framework of periodic spin-polarized density functional theory as implemented in the PWSCF code[13] with the generalized gradient approximation (GGA) and Vanderbilt ultrasoft pseudopotentials.[14] For the most stable configurations, the density functional theory with GGA+U formalism is used with $U = 6$ eV. $4 \times 4 \times 1$ and $2 \times 4 \times 1$ Monkhorst-Pack meshes are used to sample the Brillouin zone for the $\sqrt{3} \times \sqrt{3}$-$R30°$ and $4 \times \sqrt{3}$ structures, respectively. Kinetic-energy cutoffs are chosen at 25 Ry (wave function) and 200 Ry (charge). A repeated slab geometry is employed, with each slab consisting of four GaN double layers, one Ga bilayer, and Mn adatoms. The bottom surface is saturated with fractional pseudo-H atoms. An ~10.0-Å-thick vacuum separator is placed to avoid unwanted interaction between the slabs. The bottom GaN double layer and pseudo-H atoms are frozen while the other atoms are allowed to fully relax.

C. Atomic structure of the complete $\sqrt{3} \times \sqrt{3}$-$R30°$ layer

We begin our discussion with the upper limit—a fully completed $\sqrt{3} \times \sqrt{3}$-$R30°$ structure. The simplest configuration to consider is one consisting of a $\sqrt{3} \times \sqrt{3}$-$R30°$ arrangement of Mn adatoms on a Ga bilayer having a GaN-bulk-like density; we refer to this model as BL-1. However, BL-1 is quickly ruled out since the Mn adatoms are found to be unstable, sinking into the Ga layer. We next consider a model (referred to as BL-2) in which Mn atoms replace Ga atoms in a $\sqrt{3} \times \sqrt{3}$-$R30°$ arrangement within the first Ga layer (with a GaN-bulk-like density), ejecting the Ga atoms into adatom positions. A similar model was proposed by Qi *et al.* for their reported honeycomb structure.[11] But surprisingly, we find that upon relaxation, the Ga adatoms sink into the Mn-Ga layer, leading to a complete lateral atomic rearrangement.

The instability of such bulklike and adatom models leads us to a new high-density and two-dimensional model (referred to as HD-1), which is qualitatively different and found to be the most stable. As shown in Fig. 3(a), the HD-1 model consists of Mn atoms in essentially the same plane as the first Ga layer (side view), and as seen in the top view, consists of one Mn atom and three Ga atoms per $\sqrt{3}\times\sqrt{3}$-$R30°$ unit cell. This is equivalent to an average atomic density 1.33 times that of a bulklike surface. To accommodate this high atomic density,

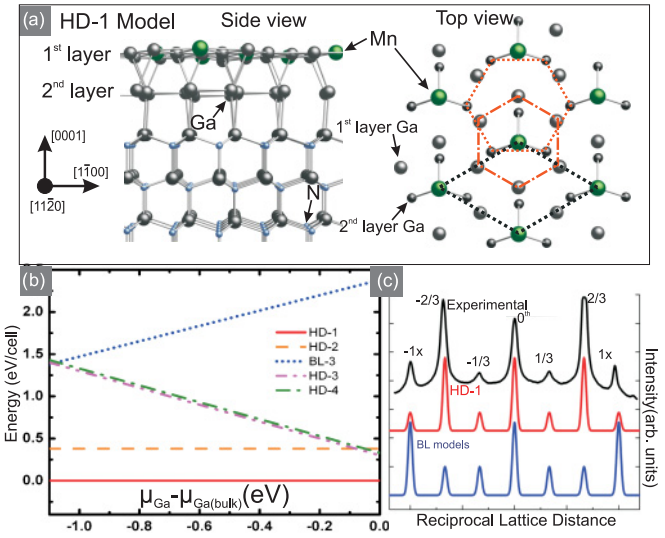

FIG. 3. (Color online) (a) Side view and top view of HD-1 model. Dashed black rhombus labels the surface unit cell. Orange hexagons (dash dotted and dotted) label the Ga configurations (first and second layers, respectively). (b) Relative formation energy calculated for five different models as a function of Ga chemical potential. The chemical potential of Ga varies between $\mu_{\mathrm{Ga(bulk)}} + \Delta H$ and $\mu_{\mathrm{Ga(bulk)}}$. The calculated values of ΔH is -0.99 eV. (c) Comparison of simulated RHEED intensity line profiles along [1$\bar{1}$00] with the experimental data.

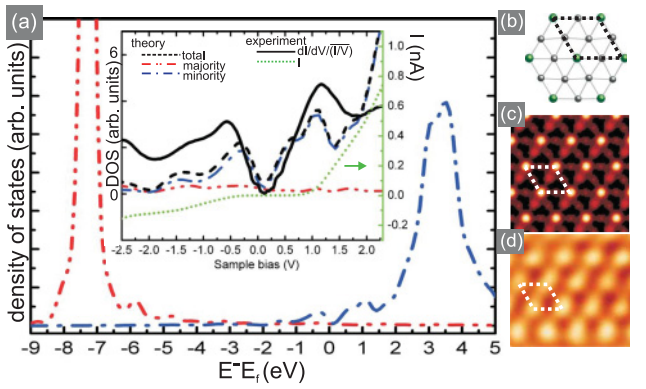

FIG. 4. (Color online) (a) Calculated spin-resolved local density of states (DOS) for Mn d electrons with $U = 6$ eV. Inset: Amplified DOS compared against normalized tunneling conductance spectrum; tunneling gap stabilized at -2 V, 0.45 nA; lock-in modulation $V_{\mathrm{mod}} = 20$ mV, $f = 3.77$ kHz. (b) HD-1 model. (c) Calculated surface density plot for $V_s = -0.1$ V. (d) Closeup STM image, $V_s = -0.1$ V, $I_t = 0.1$ nA.

Ga atoms in the first layer are drawn toward the incorporated Mn atoms and rearranged into a 30°-rotated and contracted configuration with respect to the underlying lattice. Mn sits on a near-bridge site with regard to the second-layer Ga atoms, which are buffering the 2D Mn-Ga layer from the GaN surface. The Ga-Ga and Ga-Mn spacings are calculated to be 2.6–2.8 Å, which is comparable to surface Ga-Ga spacings in the contracted bilayer model proposed for the Ga-rich GaN surface by Northrup *et al*. (2.76 Å).[10]

To compare the energetics of various models, relative formation energies are computed based on the definition by Northrup *et al*.[12] and plotted in Fig. 3(b) for five different competing models. Among these, HD-2 is similar to HD-1 as described above, except for a different Mn registry (atop site vs near-bridge site for HD-1). We explored two additional variations of HD-1 by adding one extra Ga adatom per Mn to the surface, with the Ga either neighboring a Mn (HD-3) atom or neighboring only Ga atoms (HD-4). Furthermore, we also considered a variation of BL-2 in which the Ga adatom is removed (BL-3). But as can be clearly seen from Fig. 3(b), the lowest energy among all configurations, by at least 0.3 eV, corresponds to the HD-1 model.

Further support for the HD-1 model over the BL models comes from the RHEED intensity line profiles. Nominally, a $\sqrt{3}\times\sqrt{3}$-$R30°$ structure would produce equal-intensity $3\times$ fractional streaks along [1$\bar{1}$00] and $1\times$ along [11$\bar{2}$0]. However, with the inclusion of a multiatom basis, intensity modulation will be introduced based on the well-known structure factor equation. Applying a kinematic approach, a comparison of computed line profiles is presented in Fig. 3(c) for various models. We note that all the BL models produce equal-intensity $3\times$ fractional streaks, in poor agreement with experiment, whereas the HD-1 model produces a pattern where the $\frac{2}{3}$-order streak is stronger than the $\frac{1}{3}$-order streak. Clearly, the HD-1 model results in a much better agreement with RHEED observations.

To further explore the electronic properties of the $\sqrt{3}\times\sqrt{3}$-$R30°$ structure, we applied a Hubbard-like localized U term to the density functional, a procedure known as DFT + U. This procedure is commonly used to correct for the delocalization inherent in the DFT method. In general, the U term results in a minute change in structure, but a significant change in the electronic properties. The first effect is a shifting of the majority and minority peaks outward from E_F toward larger energies. For example, the main majority peak shifts from ~ -2.3 eV for $U = 0$ eV (not shown) to ~ -7.2 eV for $U = 6$ eV [Fig. 4(a)]. The second effect is the creation of a a small dip near the Fermi level, shown more clearly in the inset to Fig. 4(a). The calculated density of states is compared directly to the normalized dI/dV spectrum, showing an excellent agreement.

Interestingly, while the tunneling conductance spectrum represents an average over multiple surface sites (including both Mn and Ga sites), the main features match very well with the Mn d electron features from the calculation. This implies that, although Mn and Ga atoms reside within essentially the same plane, Mn d electrons dominate the tunneling current. This dominance can be directly visualized in Fig. 4(c), a plot of the surface electronic density 1.5 Å from the surface, integrating over an energy window from E_F to -0.1 eV below E_F. The density plot can be directly compared to the closeup STM image shown in Fig. 4(d) taken at $V_s = -0.1$ V, showing an excellent match. Thus, we interpret the protrusions of the STM image to directly correspond to Mn atomic sites.

D. Atomic structure of the α phase and its spin ordering

We next consider the α phase in light of the HD-1 structure found for the $\sqrt{3}\times\sqrt{3}$-$R30°$. In fact, the α-phase zigzag row turns out to consist of a local $\sqrt{3}\times\sqrt{3}$-$R30°$ structure as well, as seen in the $4\times\sqrt{3}$ model shown in Fig. 5(a). Not

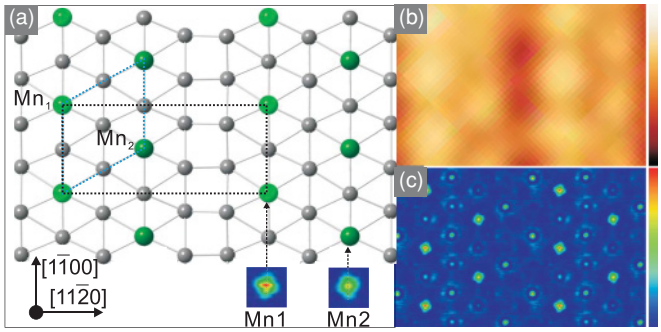

FIG. 5. (Color online) (a) Top view of $4\times\sqrt{3}$ model for the α phase. Large green spheres are surface Mn atoms and small gray spheres are surface Ga atoms. (b) Closeup STM image taken at $V_S = -0.4$ V and $I_t = 0.1$ nA. (c) Surface density plot integrated over an energy window from the Fermi level to 0.4 eV below. Note the different electronic densities for Mn_1 and Mn_2 atoms are represented by different colors closeup shown in (a)].

surprisingly, we find a high-density two-dimensional structure having Mn and Ga atoms residing in the same surface layer to be again the most energetically favorable. Moreover, the Ga atoms in the vicinity of the zigzag rows are in a contracted and rotated arrangement very similar to the HD-1 model. Within these regions, the Mn density is as high as it is for the HD-1 structure. On the other hand, the trenches between zigzag rows are devoid of Mn atoms. Figure 5(c) shows a surface density plot which is compared to a closeup STM image [Fig. 5(b)], showing that the prominent protrusions again correspond directly to the Mn sites.

Clearly then, the trench features separating the wide stripe domains (γ phase) at higher coverage [Fig. 2(d)] can also be interpreted as regions devoid of Mn. The variation in domain width observed in the experiments (4–6, 8–9, and >10 atomic rows wide) is then explained to be due to variations in the average Mn:Ga surface stoichiometry. As the Mn concentration is increased from that of the α phase (0.25 ML) toward that of a complete $\sqrt{3}\times\sqrt{3}$-$R30^\circ$ layer (0.33 ML), more Mn rows are packed into each domain, resulting in wider stripe width.

While the two Mn atoms in the $4\times\sqrt{3}$ unit cell are structurally mirror-symmetrical, one may notice an asymmetry in the constant-current STM image, namely, atom Mn_1 is shown brighter than atom Mn_2 by about 27%. This effect can be more clearly seen in the line profile inset in Fig. 2(b). Seeking to explain this asymmetry, we carried out spin-polarized calculations for the $4\times\sqrt{3}$ model, and found that a row-wise AFM configuration is energetically the most favorable compared to nonmagnetic and ferromagnetic states. In this AFM configuration, Mn_2 spins are aligned antiparallel with Mn_1 spins. Surprisingly, we find a direct influence of the spin ordering on the spin-averaged electronic structure. A small shift in the majority density of states close to the Fermi level is found between Mn_1 and Mn_2, which then results in an asymmetry in the local electronic density when integrated over a small energy window below the Fermi level. As shown more clearly in the closeup surface density plots in Fig. 5(a), Mn_1 is calculated to possess a higher electronic density compared to Mn_2. The asymmetry in the electronic density amounts to about 25% for a bias voltage of −0.4 V, in excellent agreement with the experiment.

Finally, we note that the high-density $\sqrt{3}\times\sqrt{3}$-$R30^\circ$ Mn-Ga layer provides an ideal template for $L1_0$-Mn-Ga growth. The $\sqrt{3}\times\sqrt{3}$-$R30^\circ$ unit cell is almost identical to a 2×2 supercell on the $L1_0$-Mn-Ga(111) plane.[5] We, therefore, propose that the $\sqrt{3}\times\sqrt{3}$-$R30^\circ$ structure serves as an abrupt and perfect interface for Mn-Ga epilayers on top of GaN(0001).

IV. CONCLUSIONS

To conclude, we have obtained a class of stripe-phase 2D Mn structures by depositing a submonolayer amount of Mn on GaN(0001)-1×1 surfaces at slightly elevated temperatures. Atomic models consisting of a 2D Mn-Ga surface layer in $\sqrt{3}\times\sqrt{3}$-$R30^\circ$ arrangements are derived from a combination of first-principles theory and STM observations. The surface Mn atomic sites are directly revealed by the protrusions in the STM images, due to the dominance of the Mn d electrons on the surface electronic density. Furthermore, a row-wise AFM spin ordering, reflected as an asymmetry in the spin-averaged Mn electronic states, is observed in real space for the least Mn-containing α phase. Varying the Mn concentration results in a change in the stripe width which can be expected to influence, possibly strongly, the spin ordering within the stripes. The obtained 2D structures, therefore, represent an intriguing magnetic system, as well as a promising material for studying spin injection into wide-band-gap optoelectronic devices.

ACKNOWLEDGMENTS

This study was supported by the Department of Energy, Office of Basic Energy Sciences (Grant No. DE-FG02-06ER46317) and the National Science Foundation (Grant No. 0730257). The computations were performed in the DGSCA-UNAM supercomputing center. K. K. Wang gratefully acknowledges Martin E. Kordesch for coating the substrates, and N. Takeuchi acknowledges support by Conacyt (Grant No. 48549) and DGAPA-UNAM (Grant No. IN101809).

*Present address: MPA-CINT, MS K771, Los Alamos National Laboratory, Los Alamos, NM 87545, USA.
†smitha2@ohio.edu

[1] A. Enders, R. Skomski, and J. Honolka, J. Phys. Condens. Matter **22**, 433001 (2010).
[2] M. Bode, M. Heide, K. von Bergmann, P. Ferriani, S. Heinze, G. Bihlmayer, A. Kubetzka, O. Pietzsch, S. Blügel, and R. Wiesendanger, Nature (London) **447**, 190 (2007).
[3] T. Mochizuki, R. Masutomi, and T. Okamoto, Phys. Rev. Lett. **101**, 267204 (2008).
[4] J. Honolka, T. Y. Lee, K. Kuhnke, A. Enders, R. Skomski, S. Bornemann, S. Mankovsky, J. Minár, J. Staunton, H. Ebert, M. Hessler, K. Fauth, G. Schütz, A. Buchsbaum, M. Schmid, P. Varga, and K. Kern, Phys. Rev. Lett. **102**, 067207 (2009).
[5] E. Lu, D. C. Ingram, A. R. Smith, J. W. Knepper, and F. Y. Yang, Phys. Rev. Lett. **97**, 146101 (2006).

[6]H. Kurt, K. Rode, M. Venkatesan, P. S. Stamenov, and J. M. D. Coey, Phys. Rev. B **83**, 020405 (2011).
[7]F. Wu, S. Mizukami, D. Watanabe, H. Naganuma, M. Oogane, Y. Ando, and T. Miyazaki, Appl. Phys. Lett. **94**, 122503 (2009).
[8]J. Winterlik, B. Balke, G. H. Fecher, C. Felser, M. C. M. Alves, F. Bernardi, and J. Morais, Phys. Rev. B **77**, 054406 (2008).
[9]A. R. Smith, R. M. Feenstra, D. W. Greve, M. S. Shih, M. Skowronski, J. Neugebauer, and J. E. Northrup, J. Vac. Sci. Technol. B **16**, 2242 (1998).
[10]J. E. Northrup, J. Neugebauer, R. M. Feenstra, and A. R. Smith, Phys. Rev. B **61**, 9932 (2000).
[11]Y. Qi, G. F. Sun, M. Weinert, and L. Li, Phys. Rev. B **80**, 235323 (2009).
[12]J. E. Northrup and S. B. Zhang, Phys. Rev. B **47**, 6791 (1993).
[13]S. Baroni *et al*. [http://www.democritos.it].
[14]D. Vanderbilt, Phys. Rev. B **41**, 7892 (1990).